Chapter 10

Imaging of Muscarinic Receptors in the Central Nervous System

Hideo Tsukada, Shingo Nishiyama, and Kazuhiro Takahashi

Abstract

For the quantitative imaging of muscarinic acetylcholine receptors (mAChR), we developed novel PET probes, (+)*N*-^{11}C-methyl-3-piperidyl benzilate (^{11}C-(+)3-MPB), and its *N*-alkyl substitute analogs, and evaluated them in the brains of conscious monkeys (*Macaca mulatta*) using high-resolution positron emission tomography (PET). Although (+)3-MPB had relatively poor selectivity to the subtypes of mAChR, the regional cortical distribution of ^{11}C-(+)3-MPB was found to be consistent with mAChR density in the living monkey brain as reported in vitro. In contrast, its enantiomeric analog ^{11}C-(−)3-MPB provided homogeneous distribution with no significant specific binding throughout the whole brain. The *N*-alkyl substitution of alkyl moiety from methyl (^{11}C-(+)3-MPB) to ethyl (^{11}C-(+)3-EPB) and propyl (^{11}C-(+)3-PPB) resulted in lower affinities to mAChR in vitro, the faster kinetics in the living brain, and greater sensitivity to increased endogenous ACh level, induced by acetylcholinesterase (AChE) inhibitor, than ^{11}C-(+)3-MPB. Administration of scopolamine, a mAChR antagonist, reduced ^{11}C-(+)3-MPB binding to mAChR in all regions except the cerebellum, and the reduction of ^{11}C-(+)3-MPB uptake was well correlated with the degree of impairment of working memory performance assessed in conscious monkeys. These results demonstrated that PET imaging with ^{11}C-(+)3-MPB could be useful for diagnosis of neurological diseases associated with impaired mAChR function and cognitive function.

Key words Brain, Muscarinic acetylcholine receptor, ^{11}C-(+)3-MPB, PET

1 Introduction

In the cholinergic neuronal system, acetylcholine (ACh) is the primary neurotransmitter released in the central nervous system (CNS). The cholinergic receptor (AChR) population is divided into nicotinic and muscarinic subclasses, and the AChR appears to be predominantly of the muscarinic-type receptor (mAChR) in the CNS. The mAChR belongs to the family of receptors coupled to heterotrimeric GTP-binding proteins (G-proteins), and the CNS mAChR system plays an important role in memory and cognitive functions. Alzheimer-type dementia (AD) has been neuropathologically characterized by the presence of neurofibrillary tangles with the deposition of hyperphosphorylated tau protein inside nerve cells

Jaromir Myslivecek and Jan Jakubik (eds.), *Muscarinic Receptor: From Structure to Animal Models*, Neuromethods, vol. 107,
DOI 10.1007/978-1-4939-2858-3_10,

and senile plaques with extracellular aggregation of amyloid-β (Aβ) protein [1, 2]. Moreover, loss of cholinergic neurons in the forebrain [3], reduced cholinergic activity in the hippocampus and cortical loss of choline acetyltransferase [4], and reduced central mAChR binding have been observed in the brains of AD patients [5–7]. In addition, the severity of these cholinergic abnormalities is closely correlated with the degree of dementia [6, 7].

Positron emission tomography (PET) has been applied for noninvasive investigations of physiological functions as well as neurodegenerative dysfunctions of mAChR in the living brain. Several antagonist-based ^{11}C-labeled-PET probes for imaging of mAChR in the CNS have been developed and evaluated, including ^{11}C-scopolamine [8–10], ^{11}C-dexetimide [11], ^{11}C-quinuclidinyl benzilate (QNB) [12], ^{11}C-benztropine [13], and ^{11}C-tropanyl benzilate (TRB) [14, 15]. These labeled ligands for mAChR, however, show poor subtype selectivity, relatively low uptake to the brain, and also slow dissociation rates from the binding sites which may limit quantitative measurement of the density of mAChR in vivo [15]. A low dissociation rate from mAChR makes analysis difficult, because a true equilibrium state cannot be obtained within the PET scanning time with the short half-lives of positron emitters. To solve these problems, a radiolabeled mAChR probe, *N*-^{11}C-methyl-4-piperidyl benzilate (^{11}C-4-MPB) (Fig. 1), with more favorable kinetic properties than previous compounds was proposed [16]. However, the properties of ^{11}C-4-MPB with

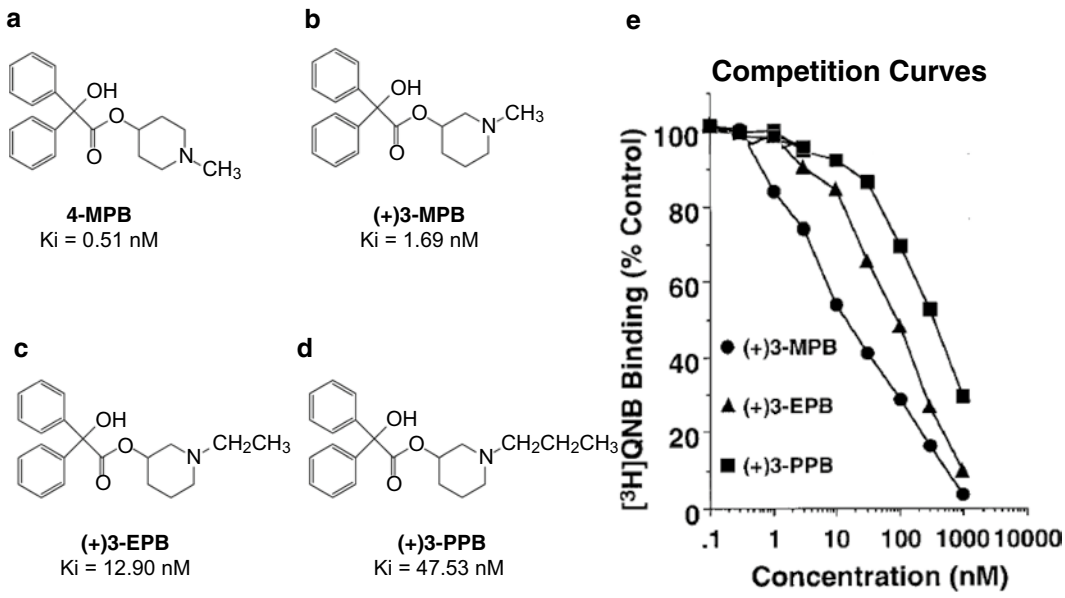

Fig. 1 Chemical structures of 4-MPB (**a**), (+)3-MPB (**b**) and its *N*-alkyl substitution analogs, (+)3-EPB (**c**) and (+)3-PPB (**d**). Affinity (K_i) values of each compound were determined by in vitro competitive assay in rat brain slices with ^{3}H-QNB, as shown in **e**

relatively high affinity to mAChR were still insufficient for quantitative imaging of mAChR in the living brain. In 1997, we proposed a novel mAChR probe, *N*-^{11}C-methyl-3-piperidyl benzilate (^{11}C-3-MPB) [17] (Fig. 1). Since its chemical structure contained a chiral carbon, it provides two stereoisomers, an active form is ^{11}C-(+)3-MPB and an inactive one is ^{11}C-(−)3-MPB. Active form, ^{11}C-(+)3-MPB, revealed relatively low affinity to mAChR as determined by in vitro binding assay [17, 18]. Furthermore, ^{11}C-(+)3-MPB was evaluated for the quantification of cerebral mAChR binding in the brain of conscious monkey (*Macaca mulatta*) [19]. By comparison between young and aged monkeys changes in ^{11}C-(+)3-MPB binding to mAChR were found [20, 21]. The temporal relationship between the occupancy level of central mAChR by scopolamine, as measured by ^{11}C-(+)3-MPB, and cognitive impairment, as assessed by the delayed matching-to-sample, was determined in conscious monkeys [22].

This chapter will provide a detailed overview of the development of a novel PET probe, ^{11}C-3-MPB, for mAChR imaging from design of its chemical structure, synthesis, radiolabeling to its assessments in vitro as well as in vivo on experimental animals.

2 Materials and Methods

2.1 Syntheses of Cold 3-PB, 3-MPB, 4-PB, and 4-MPB

It is well known that stereoisomers exhibit different properties in target-binding affinity/specificity, which results in their different pharmacological properties. To apply the chemical compounds with stereoisomers like 3-MPB as PET probe agents, quality control of enantiomeric purity is a very critical factor in the production of their corresponding precursors to radiolabeling.

As a precursor of ^{11}C-3-MPB, 3-piperidyl benzilate (3-PB) was prepared following a previously reported procedure [17]. A mixture of benzene (30 mg), 3-piperidinol (0.4 g), and methyl benzilate (1.0 g) was stirred and heated to reflux in a flask with a Molecular Sieve 4A column, a reflux condenser, and a soda lime tube. When all methyl benzilate was dissolved, sodium methoxide (20 mg) was added to the flask. After 3-h reaction, the reaction mixture was cooled down to room temperature, and 50 ml of 1 mol/l hydrochloric acid was added for separation into two phases. The aqueous phase was washed twice with 50 ml of ether, and made the phase basic with ammonium hydroxide to precipitate the benzyl ester. Thirty milliliters of ether was added twice to the aqueous phase to dissolve the benzyl ester and separate the ether layer. The ether layer was washed twice with water, dried with anhydrous potassium carbonate, filtered, and then the solvent was removed by distraction in vacuum. The residue was crystallized in ether-hexane solution, and the solid was separated by filtration as enantiomeric 3-PB. (+)3-PB and (−)3-PB were separated using an

HPLC system with a chiral column (Chiralcel OJ column, Daiseru Corporation, Osaka, Japan) eluted with a mixture of hexane/ethanol = 80/20 (v/v) under a flow rate of 0.5 ml/min. The retention times of (+)3-PB and (−)3-PB were 27.0 min and 16.8 min, respectively.

As the standard compound of ^{11}C-3-MPB for quality control analysis, 3-MPB was obtained using *N*-methyl-3-piperidinol (0.45 g) instead of 3-piperidinol by the same reaction as 3-PB synthesis described above. (+)3-MPB and (−)3-MPB were isolated using same HPLC system used in (+) and (−)3-PB isolation. The retention times of (+)3-MPB and (−)3-MPB were 15.8 min and 13.2 min, respectively.

For the comparison, 4-piperidyl benzilate (4-PB) and 4-methylpiperidyl benzilate (4-MPB) were prepared according to a previously reported method [23]. A mixture of benzene (30 mg), 4-piperidinol (0.4 g), and methyl benzilate (1.0 g) was stirred and heated to reflux in a flask with a Molecular Sieve 4A column, a reflux condenser, and a soda lime tube. When all methyl benzilate was dissolved, sodium methoxide (20 mg) was added to the flask. After 3 h reaction, the reaction mixture was cooled down to room temperature, and 50 ml of 1 mol/l hydrochloric acid was added for separation into two phases. The aqueous phase was washed twice with 50 ml of ether, and the phase was made basic with ammonium hydroxide to precipitate the benzyl ester. Thirty milliliters of ether was added twice to the aqueous phase to dissolve the benzyl ester and separate the ether layer. The ether layer was washed twice with water, dried with anhydrous potassium carbonate, filtered, and then the solvent was removed by distraction in vacuum. The residue was crystallized in ether-hexane solution, and the solid was separated by filtration as enantiomeric 4-PB. 4-MPB was obtained using *N*-methyl-4-piperidinol (0.45 g) instead of 4-piperidinol by the same reaction as 4-PB synthesis described above.

2.2 In Vitro Assessment of Novel PET Probes

The binding affinity of each probe was assessed by a competitive binding assay in rat brain slices using ^{3}H-QNB autoradiography. Since it is generally considered that the information derived from autoradiography is more pertinent to the in vivo properties of the receptor than that obtained from "pure" binding studies carried out using cell-free preparations, we applied this method for PET imaging agents.

The frozen brain was sectioned on a Cryostat (CM3000, Leica Microsystems, Nussloch, Germany) into 10 μm coronal tissue sections (bregma −2.3 to −2.8 mm), which were transferred onto cooled, gelatinized glass slides. The cryosections were incubated with ^{3}H-QNB (1.2 nM) and varying amounts of each PET probe for 30 min at 25 °C in Tris–HCl buffer. Nonspecific binding of the radioligand in the brain slice was determined by including a

saturating concentration (1 μM) of atropine in the incubation medium. The incubation was terminated by rinsing the sections twice for 2 min each in cold buffer, then dipping briefly in cold distilled water (4 °C), and slides were dried rapidly on a hot-plate (50 °C). The labeled slices were exposed for 3 days to an imaging plate (TR-2040, Fuji Film Co., Tokyo, Japan), and the imaging data were analyzed (BAS-2500, Fuji Film Co., Tokyo, Japan). Specific binding of ^{3}H-QNB was estimated as the difference between total binding and nonspecific binding. Specific binding was plotted against the concentration of each ligand to determine concentration causing 50 % inhibition (IC_{50} values), which were converted to inhibition constants (K_i) using the Cheng and Prusoff equation [24]. The rat brain anatomical structures in autoradiographic images were visually identified according to the atlas of Paxinos and Watson [25].

Subtype specificity of (+)3-MPB and 4-MPB was assessed using human mAChRs (M_1–M_5) transfected in CHO-K1 cells (Receptor Biology, Inc., Beltsville, USA) [26]. For the experiments, the membranes were thawed and diluted in phosphate-buffered saline (PBS, pH 7.4) and homogenized in a glass vessel with the aid of a Teflon pestle. The final concentration of receptors in the assay was in the range of 50–100 pM. For the association study, homogenate was incubated with labeled compound at 22 °C, and the binding was started at different time points in reverse order and terminated simultaneously in all samples at time 0. The incubation was terminated by rapid filtration through Whatman GF/B glass fiber filters (FPB-148, Gaithersburg, USA). For the dissociation study, the association of samples was terminated after 50 min. The dissociation was started by adding unlabeled compound in excess at different time points, and the reactions were terminated simultaneously in all samples at time 0. After termination of the incubation, the filters were rinsed four times with 2 ml of ice-cold incubation buffer each time. Thereafter, the filter rings were collected from the cell harvester (Brandel, Gaithersburg, USA) and were transferred into vials for counting in a γ-counter.

To measure lipophilicity of the labeled ligands, their partition coefficients (log *D* at pH 7.4) were measured. Octanol (2 ml) and 0.066 M phosphate-buffer, pH 7.4 (2 ml) were mixed for 3 min. Ten milliliters of each labeled compound was mixed, vortexed for 3 min, centrifuged for 5 min, separated, and ^{11}C-radioactivity was counted. The lipophilicity of each labeled PET probe was then calculated as logarithm of the distribution constant between lipophilic organic (octanol) phase and polar aqueous (water) phase.

The buffer solutions can be stored conveniently at 4 °C and are stable for several months. Drug solutions and radioligands are distributed in small aliquots and stored at –20 °C. Atropine solutions are prepared fresh monthly.

2.3 Radiosynthesis of ^{11}C-(+)3-MPB, ^{11}C-(–)3-MPB, and ^{11}C-4-MPB

Carbon-11 (^{11}C), a positron emitter with a 20 min half-life, is a candidate for the isotopic or non-isotopic labeling of any organic compound used for PET imaging. In isotopic labeling, since ^{11}C replaces stable ^{12}C/^{13}C in the molecule, the biological properties of the molecule are virtually unchanged. In non-isotopic labeling, a group containing ^{11}C is added to the molecule of interest, producing a new compound with different properties to the original.

The reaction time with ^{11}C that has a short-half life (=20 min) needs to be as short as possible, and the reaction needs to be driven to give useful yields within one physical half-life. Reactions are promoted by (1) using a large excess of precursor to consume labeling agent; (2) using a high precursor concentration in small volumes; (3) using sealed vessels for elevated reaction temperature; and (4) using microwaves or sonication. In addition, since the stability of some ^{11}C-PET probes was low even at the end of synthesis (EOS) because of a radiolysis, this should be taken into account by suppressing radiolysis by adding a selective scavenger for hydroxyl radicals and/or hydrated electrons into the PET probe solution.

The concentration of ^{11}C-labeled probe was calculated from calibration curves by simultaneous monitoring of radioactivity and UV absorbance with authentic substances used as standards. Specific radioactivity of ^{11}C-labeled probe was defined as the ratio of radioactivity (Ci) to accompanying cold compound (mol), and was expressed in units of Ci/mol. There is substantial dilution of ^{11}C-labeled compound with cold compound. The amount of cold compound remains constant, while the radioactivity decays over time according to the half-life of the positron emitter. Therefore, the specific radioactivity for PET probe should be cited with respect to a particular time, such as the end of radionuclide production (EOB), EOS, or time of injection (TOI).

Positron emitting carbon-11 (^{11}C) was produced by a ^{14}N(p,a)^{11}C nuclear reaction using a cyclotron (HM-18; Sumitomo Heavy Industry, Tokyo, Japan) at Hamamatsu Photonics PET center and obtained as ^{11}C-CO_2. Labeled compounds were synthesized using a modified CUPID system (Sumitomo Heavy Industry, Tokyo, Japan). As isotopic labeling, ^{11}C-(+)3-MPB and its stereoisomer ^{11}C-(–)3-MPB were labeled by *N*-methylation of respective nor-compounds ((+)3-PB or (–)3-PB) with ^{11}C-methyl iodide (Fig. 2) [17, 19]. ^{11}C-CO_2 was converted to ^{11}C-methyl iodide by $LiAlH_4$ reduction followed by reaction with HI, and ^{11}C-methyl iodide was trapped in a reaction vial containing the free base (+) or (–)3-PB (0.5 mg) in DMF (200 μL) at –40 °C. When reaching the maximum radioactivity of ^{11}C-methyl iodide, the vial was hearted at 80 °C for 5 min. After cooling down, the reaction mixture was injected into an HPLC system with a C18 column (μBondapak-C18, Waters, Milford, MA) eluted with a mixture of acetonitrile/0.1 M AcONa/Acetic acid = 700/300/1 (v/v) under a flow rate of 7 ml/min. The fraction eluted at a retention time of ca. 10 min was transferred to an

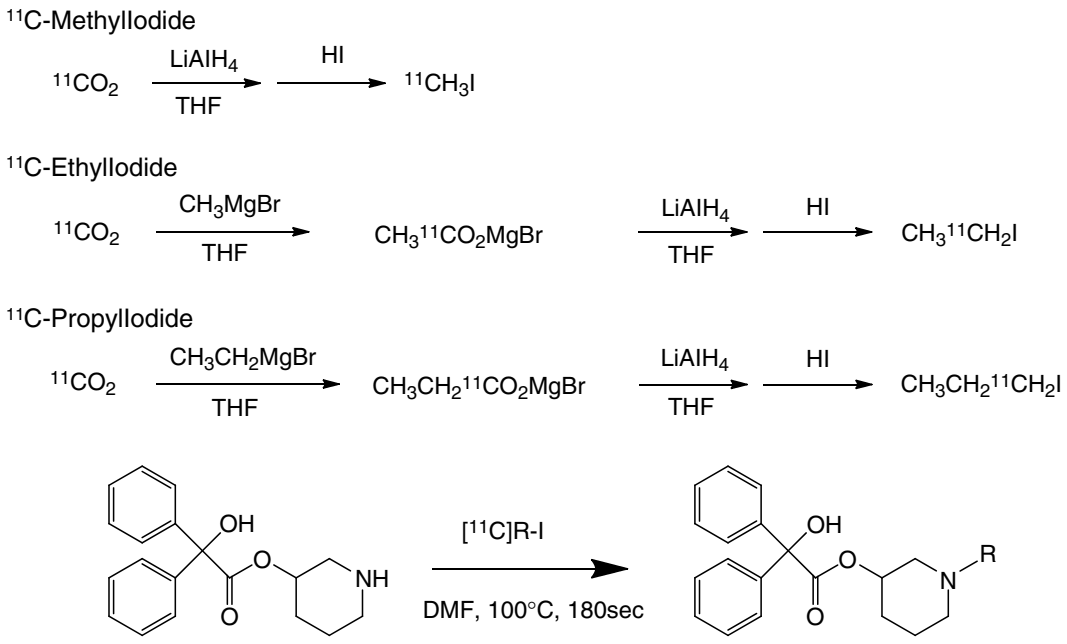

Fig. 2 Radiolabeling of ^{11}C-(+)3-MPB, ^{11}C-(+)3-EPB, and ^{11}C-(+)3-PPB using (+)3-PB and ^{11}C-methyl iodide, ^{11}C-ethyl iodide, and ^{11}C-propyl iodide, respectively

evaporator for evaporation of elute solvent, dissolved in saline (10 ml), and filtered through a 0.22-μm pore size filter.

Chemical and radiochemical analysis of ^{11}C-(+)3-MPB and ^{11}C-(−)3-MPB was performed by HPLC in a system consisting of a column (Finepak SIL C18-S, 4.6 mm in diameter × 150 mm in length, Jasco, Tokyo, Japan), pump (CCPS, Tosoh, Tokyo, Japan), UV detector (UV-8020, Tosoh, Tokyo, Japan), and radio detector (RLC-700, Hitachi Aloka Medical, Inc., Tokyo, Japan) using CH_3CN/30 mM CH_3COONH_4/CH_3COOH (350/650/2) as a mobile phase at a flow rate of 1 ml/min. Analyses of the enantiomeric purity of ^{11}C-(+)-3-MPB and ^{11}C-(−)-3-MPB were performed by HPLC in a system consisting of a column (Chirobiotic V, 4.6 × 250 mm, Astec, NJ, USA), pump (DP8020, Tosoh, Tokyo, Japan), UV detector (UV-8020, Tosoh, Tokyo, Japan), and radio detector (TCS-713, Aloka, Tokyo, Japan) using CH_3OH/CH_3COOH/$(C_2H_5)_3N$ (1000/0.5/0.1) as a mobile phase at a flow rate of 1 ml/min. The retention times of ^{11}C-(+)3-MPB and ^{11}C-(−)3-MPB were 15.8 min and 13.2 min, respectively, both of which were identical to each corresponding standard compound.

The radioactive purity of each labeled compound used in this study was greater than 99 % and the specific radioactivity ranged from 61.7 to 92.4 GBq/μmol for ^{11}C-(+)3-MPB, and from 60.0 to 79.5 GBq/μmol for ^{11}C-(−)3-MPB at EOS. Enantiomeric purity of ^{11}C-(+)-3-MPB and ^{11}C-(−)-3-MPB was 100 %.

As for the previously reported reference, ^{11}C-4-MPB was prepared by the same method as used for ^{11}C-3-MPB labeling. The radioactive purity used in this study was greater than 99 % and the specific radioactivity ranged from 34.4 to 75.9 GBq/μmol for ^{11}C-4-MPB at EOS.

2.4 Radiosynthesis of ^{11}C-(+)3-EPB and ^{11}C-(+)3- PPB

In order to evaluate the effects of affinity to mAChR on kinetics as well as the sensitivity to changes in the synaptic endogenous ACh level, two *N*-alkyl substitution analogs of ^{11}C-(+)3-MPB, *N-11C-ethyl*-3-piperidyl benzilate (^{11}C-(+)3-EPB) and *N*-^{11}C-propyl-3-piperidyl benzilate (^{11}C-(+)3-PPB), were used [18]. Standard compounds, (+)3-EPB and (+)3-PPB, were synthesized by *N*-ethylation and *N*-propylation, respectively, of (+)3-PB. For the radiolabeling, C-11 was produced by ^{14}N(p,a)^{11}C nuclear reaction using a cyclotron (HM-18; Sumitomo Heavy Industry, Tokyo, Japan) and obtained as ^{11}C-CO_2. Labeled compounds were synthesized using a modified CUPID system (Sumitomo Heavy Industry, Tokyo, Japan). Instead of ^{11}C-methyl iodide, ^{11}C-ethyl iodide or ^{11}C-propyl iodide was prepared by reaction of Grignard reagent (Fig. 2) [18, 27]. In the synthesis of ^{11}C-ethyl iodide or ^{11}C-propyl iodide, 0.5 ml of 0.25 M methylmagnesium bromide in tetrahydrofuran (THF) or 0.5 ml of 0.25 M ethylmagnesium bromide in THF were used. After a reaction time for 5 min, 1 ml of lithium aluminum hydrate (1 M) in THF was added and the solvents were removed. Two milliliters of hydriodic acid (54 %) was then added, and the product was distilled off and transferred in a stream of nitrogen gas through a drying tower containing sodium hydroxide/phosphorus pentoxide to the reaction vessel. ^{11}C-(+)3-EPB or ^{11}C-(+)3-PPB was synthesized by *N*-ethylation or *N*-propylation of (+)3-PB with ^{11}C-ethyl iodide or ^{11}C-propyl iodide.

Chemical and radiochemical analysis of ^{11}C-(+)3-EPB and ^{11}C-(+)3-PPB was performed by HPLC in a system consisting of a column (Finepak SIL C18-S, 4.6 mm in diameter × 150 mm in length, Jasco, Tokyo, Japan), pump (CCPS, Tosoh, Tokyo, Japan), UV detector (UV-8020, Tosoh, Tokyo, Japan), and radio detector (RLC-700, Hitachi Aloka Medical, Inc., Tokyo, Japan) using CH_3CN/30 mM CH_3COONH_4/CH_3COOH (350/650/2) as a mobile phase at a flow rate of 1 ml/min. Analyses of the enantiomeric purity of ^{11}C-(+)-3-EPB and ^{11}C-(+)-3-PPB were performed by HPLC in a system consisting of a column (Chirobiotic V, 4.6 × 250 mm, Astec, NJ, USA), pump (DP8020, Tosoh, Tokyo, Japan), UV detector (UV-8020, Tosoh, Tokyo, Japan), and radio detector (TCS-713, Aloka, Tokyo, Japan) using CH_3OH/CH_3COOH/$(C_2H_5)_3N$ (1000/0.5/0.1) as a mobile phase at a flow rate of 1 ml/min. The retention times of ^{11}C-(+)3-EPB, ^{11}C-(−)3-EPB, ^{11}C-(+)3-PPB, and ^{11}C-(−)3-PPB were 15.3 min, 14.8 min, 12.7 min, and 13.7 min, respectively.

The radioactive purity of each labeled compound used in this study was greater than 99 %, and the specific radioactivity ranged from 34.1 (^{11}C-(+)3-PPB) to 66.3 GBq/μmol (^{11}C-(+)3-EPB) at EOS. The specific radioactivity levels of these two PET probes were comparable to that of ^{11}C-(+)3-MPB. Enantiomeric purity of ^{11}C-(+)-3-EPB and ^{11}C-(+)-3-PPB were 100 %.The solution of labeled compound was passed through a 0.22-μm pore size filter before intravenous administration to the subjects.

For the assessment of acetylcholinesterase (AChE) level in the living brain using PET, *N*-^{11}C-methyl-4-piperidyl acetate (^{11}C-MP4A) was labeled by *N*-methylation of its corresponding nor-compound, 4-piperidyl acetate (P4A) (ABX Advanced Biochemical Compounds, Radeberg, Germany), with ^{11}C-methyl iodide [28].

2.5 MRI Data Acquisition

Magnetic resonance images (MRI) of the monkeys were obtained with a 3.0 T MR imager (Signa Excite HDxt 3.0 T, GE Healthcare Japan, Tokyo, Japan) using a 3D-Spoiled Gradient Echo (SPGR) sequence (176 slices with a 256×256 image matrix, slice thickness/spacing of 1.4/0.7 mm, TE: 3.4–3.6 ms, TR: 7.7–8.0 ms, TI: 400 ms, and flip angle: 15°) under pentobarbital anesthesia.

2.6 PET Analysis

The PET studies in this chapter have been conducted with monkeys under conscious condition. Anesthetics have been used in non-human primate PET studies, because it is necessary to fix the animal during PET scanning. However, anesthetics have been reported to affect several neuronal functions, resulting in an alteration of neuronal activities in the central nervous system. Thus, the brain function as well as the pharmacological actions as measured by PET should be affected by anesthetics [29–32]. In order to avoid these anesthetic effects, we developed a PET system with transaxial resolution of 2.6 mm full width at half maximum (FWHM) and a center-to-center distance of 3.6 mm (SHR-7700, Hamamatsu Photonics, Hamamatsu, Japan) [33], and its gantry can be tilted up to 90° for brain imaging of monkey sitting on a monkey chair under conscious condition. In order to eliminate the stress caused by head motion restriction influence on measured parameters, as reported in the dopaminergic neuronal system [34], the monkeys were trained for more than 2 months and plasma cortisol was monitored.

After an overnight fast, a monkey (*Macaca mulatta*) was seated on a monkey chair under conscious condition and fixed with stereotactic coordinates aligned parallel to the orbitomeatal (OM) line. After a transmission scan for 30 min using a ^{68}Ge-^{68}Ga rotation rod source, an emission scan for 91 min was conducted after the injection of each labeled compound (100–120 MBq/kg body weight) through the venous cannula.

The PET data obtained were reconstructed by the filtered back projection (FBP) method with a Hanning filter of 4.5 mm FWHM. Volumes of interest (VOIs) in brain regions were drawn manually on the MRI referring regional information from BrainMaps.org, and VOIs of MRI were superimposed on the co-registered PET images to measure the time activity curves (TACs) of each PET probes for kinetic analysis.

For quantitative analysis of ^{11}C-(+)3-MPB, arterial blood samples were obtained every 8 s up to 64 s, followed by 90 and 150 s, and then 4, 6, 10, 20, 30, 45, 60, and 90 min after tracer injection, and the blood samples were centrifuged to separate plasma, weighed, and their radioactivity was measured. For metabolite analysis, methanol was added to some plasma samples (sample/methanol = 1/1) obtained at 16, 40, and 64 s, 6, 10, 30, and 45 min after the injection, followed by centrifugation. The obtained supernatants were developed using thin layer chromatography plates (AL SIL G/UV, Whatman, Kent, UK) with a mobile phase of ethyl acetate. The ratio of unmetabolized fraction was determined using a phosphor imaging plate (FLA-7000, Fuji Film, Tokyo, Japan). The input function of unmetabolized ^{11}C-(+)3-MPB was calculated using the data obtained by correction of the ratio of the unmetabolized fraction to total radioactivity, which was used as the arterial input function.

Logan [35] and Patlak [36] graphical analyses with metabolite-corrected plasma input were applied for quantitative measurements of ^{11}C-(+)3-MPB binding to mAChR in the living brain using PMOD software (PMOD Technologies Ltd., Zurich, Switzerland). The Logan graphical plot [35] directly gives a linear function of the free receptor concentration known as the distribution volume based on the following Eq. (1):

$$\int \mathrm{ROI}(t)\,\mathrm{d}t \,/\, \mathrm{ROI}(T) = \mathrm{DV} \int \mathrm{Cp}(t)\,\mathrm{d}t \,/\, \mathrm{ROI}(T) + C$$

where ROI(T) and Cp(T) represent tissue and metabolite-corrected arterial plasma radioactivity, respectively, at time T, DV is the slope and C is the intercept on the Y-axis. For the reversibly labeled compounds, this Logan plot becomes linear after some time with a slope (DV) that is equal to the steady-state distribution volume. The ratios of DV in each ROI (DV(ROI)) to K in the cerebellum (DV(CE)) were calculated to determine the distribution of mAChR in the living brain.

Patlak plot analysis [36] was used to measure the net accumulation of PET probe in the irreversible compartment based on the following Eq. (2):

$$\int \mathrm{ROI}(t)\,\mathrm{d}t \,/\, \mathrm{Cp}(T) = \mathrm{DV} \int \mathrm{Cp}(t)\,\mathrm{d}t \,/\, \mathrm{ROI}(T) + C$$

where ROI(T) and Cp(T) represent tissue and metabolite-corrected arterial plasma radioactivity, respectively, at time T, DV is the slope, and C is the intercept of the Y-axis. The slope (DV) was equal the parameter combination $K_1k_3/(k_2+k_3)$. The dissociation constant (k_4) is assumed to be negligible over the course of the scan. Patlak slope value is influenced by the blood–brain barrier (BBB), transport rate constants (K_1 and k_2), and thus does not provide a pure estimate of association constant (k_3).

2.7 Drug Perturbations on PET Probe Binding to mAChR

A PET probe is no-cold added (NCA) when no source of cold compound has been added deliberately during its production. In contrast, it is cold-added (CA) when a source of cold compound has been added deliberately during its production.

For the inhibition study of ^{11}C-(+)3-MPB binding to mAChR in the living brain, scopolamine, a specific mAChR antagonist, was administered at a dose of 50 μg/kg 30 min before PET probe injection under NCA condition.

In order to evaluate the sensitivity to changes in the synaptic endogenous ACh level induced by AChE inhibition, Aricept, an AChE inhibitor, was intravenously administered at doses of 50 and 250 μg/kg 30 min before ^{11}C-(+)3-MPB injection under NCA condition.

To determine the correlation between mAChR occupancy and cognitive impairment in monkeys, scopolamine was administered at the dose of 10 and 30 μg/kg, and then PET measurements with ^{11}C-(+)3-MPB injection under NCA condition and cognitive performance test were serially conducted 2, 6, 24 and 48 h after administration of scopolamine. The mAChR occupancy levels were determined from the degree of reduction (%) of the BP_{ND} by scopolamine as following Eq. (3):

$$\text{Occupancy}(\%) = \left(1 - BP_{ND}\text{post}(\text{ROI}) - BP_{ND}\text{pre}(\text{ROI})\right) \times 100$$

where BP_{ND}pre(ROI) and BP_{ND}post(ROI) are BP_{ND} pre- and post-scopolamine, respectively.

2.8 Effects of Aging on mAChR

Several clinical PET studies have attempted to determine quantitatively the age-related alterations of mAChR in the living brain using ^{11}C-benztropine [37], ^{11}C-4-MPB [38–40], and ^{11}C-TBZ [41]. These PET probes for mAChR, however, showed relatively low uptake to the brain and also slow dissociation rates from mAChR, which may limit estimation of the density of binding sites in vivo [15]. Therefore, we attempted to assess the age-related changes in mAChR with ^{11}C-(+)3-MPB, a reversible-type PET probe, in the living brains of young (ca. 6 years old) and aged (ca. 20 years old) monkeys in a conscious state [20]. The syntheses of ^{11}C-(+)3-MPB, PET data acquisitions, and the analysis of cortical TAC were conducted as described in Sections 2.3 and 2.5.

Saturation experiments were performed to examine the effects of aging on in vivo binding parameters (maximum binding capacity B_{MAX} and equilibrium dissociation constant K_D) of ^{11}C-(+)3-MPB as performed previously in the dopaminergic system [42, 43]. ^{11}C-(+)3-MPB was injected into monkeys under NCA and CA conditions and together with various amounts cold (+)3-MPB from 3 to 300 μg/kg. The total radioligand concentration of ^{11}C-(+)3-MPB in the cerebellum was used as an estimate of the free radioligand concentration (F) in each ROI. Specific binding (B) was defined as radioactivity in each ROI reduced by F. The curve for B was fitted to a set of three exponential functions to determine the time point at which B reached a peak. The values for B and F at these time points were used in the in vivo pseudo Scatchard plot analysis where the ratio of B/F was plotted against B [44]. The apparent in vivo B_{MAX} and K_D values were calculated using LIGAND software.

2.9 Cognitive Assessment of Monkeys

Although it had been well known that blockade of mAChR with scopolamine, a specific mAChR antagonist, resulted in transient cognitive impairment [45], there have been no study revealing the relationship between the occupancy level of central mAChRs and the degree of cognitive impairment induced by scopolamine in primates. Therefore, we attempted to evaluate the correlation between the mAChR occupancy level and cognitive impairment in conscious monkeys [22].

Cognitive impairment was determined by a titration version of delayed match to sample (T-DMS) task [46]. DMS task is one method for evaluating potential drug effects on cognitive functions. Typically, a sample visual stimulus is presented to the animal for a short period. Following a delay, the sample and another test stimulus are presented simultaneously. The subject is required to choose the sample visual stimulus in order to be rewarded. However, one limitation of the conventional DMS task is that the maximal delay is fixed for all subjects, although cognitive abilities differ among them. With T-DMS task test, under control condition, the monkeys' correct response levels depend on each animal's working memory capacity as determined by the maximal delay interval.

Sixty-four different visual stimuli comprising all combinations of eight distinct colors and eight distinct shapes were presented on a touch-sensitive screen placed in front of monkey. A sample stimulus appeared for 300 ms, disappeared, and then the sample stimulus and three other stimuli appeared after a delay. Monkeys were trained to touch the visual stimulus that matched the sample within 5 s, and if the answer was correct, water drops (0.2 ml) were given as a reward. If the trial was correct, the next trial was presented with a delay 1 s longer. The delay for the trial after an incorrect choice was decreased by 1 s. This process was repeated until the delay for a correct choice peaked, the delay interval over the last

ten trials of each session was used as the cognitive index. Cognitive impairment was defined as following Eq. (4):

$$\text{Cognitive Impairment}\,(\%) = \left(1 - \text{Cognitive Index}_{\text{post}} - \text{Cognitive Index}_{\text{pre}}\right) \times 100$$

where Cognitive $\text{Index}_{\text{pre}}$ and Cognitive $\text{Index}_{\text{post}}$ are pre- and post-administration values for vehicle or scopolamine, respectively.

PET measurements and cognitive performance test were serially conducted 2, 6, 24, and 48 h after administration of scopolamine, and the degrees of impaired of cognitive function were plotted against mAChR occupancy degrees induced by scopolamine administration.

3 Experimental Results

3.1 In Vitro Assessment of (+)3-MPB Analogs

Synthesized 3-PB, 3-MPB, 3-EPB, and 3-PPB were analyzed to confirm their chemical structures as ^{1}H-NMR spectra (R-1200, Hitachi High-Tech Fielding Corporation, Tokyo, Japan). $^{1H\text{-}NMR}$ of 3-PB: 7.36 (m, 10H), 4.92 (m, 1H), 2.94 (m, 1H), 2.70 (m, 4H), 1.82 (m, 1H), 1.71 (m, 1H), 1.26 (m, 1H). 3-MPB: 7.36 (s, 10H), 5.02 (m, 1H), 2.69 (m, 1H), 2.46 (m, 1H), 2.24 (s, 3H), 2.17 (m, 1H), 1.94 (m, 1H), 1.82 (m, 1H), 1.71 (m, 1H), 1.58 (m, 1H), 1.41 (m, 1H), 1.26 (m, 1H); 3-EPB: 7.32 (s, 10H), 5.01 (m, 1H), 4.41 (s, 1H), 2.72 (m, 2H), 2.25 (m, 4H), 1.68 (m, 3H), 1.25 (s, 1H), 0.97 (t, 3H); 3-PPB: 7.36 (s, 10H), 5.01 (m, 1H), 4.37 (s, 1H), 2.74 (m, 2H), 2.27 (m, 4H), 1.60 (m, 6H), 0.92 (t, 3H).

As shown in Fig. 1, we designed methods to synthesize several analogs of (+)3-MPB, and evaluated their affinities to mAChR and lipophilicity. In competition assays with ^{3}H-QNB, the IC_{50} and Ki values of (+)3-MPB, (+)3-EPB, (+)3-PPB, and their inactive stereoisomers, (−)3-MPB, (−)3-EPB, and (−)3-PPB, for mAChR were determined using rat brain slices in vitro. Since the binding of ^{3}H-QNB showed a time-dependent increase, reaching equilibrium by about 30 min, an incubation time of 30 min was chosen for this competition assays. As a result, (+)3-MPB had the highest (K_i = 1.69 nM), (+)3-EPB had moderate (12.90 nM), and (+)3-PPB had the lowest affinity (47.53 nM) for mAChR in the neocortex of the rat brain (Fig. 1e), suggesting that the longer alkyl chain length caused the lower affinity [47]. The affinity of 4-MPB (0.51 nM) was 3.3-fold higher than that of (+)3-MPB. In contrast, (−)3MPB, (−)3-EPB, and (−)3-PPB showed remarkably lower affinity to the mAChR (1000 nM and more), which were two orders lower than those of their corresponding active (+) forms [18]. The log D at pH 7.4 of ^{11}C-(+)3-MPB, ^{11}C-(+)3-EPB, and ^{11}C-(+)3-PPB were 1.53, 1.68, and 2.37, respectively.

By using the five cloned human mACh receptors, the K_D values for (+)3-MPB exhibited no significant selectivity for any

subtype, whereas the binding profile of K_i values for (+)3-MPB was $M_4 \geq M_1 > M_3 \geq M_2 > M_5$. A binding profile for 4-MPB was $M_4 > M_1 \geq M_3 \geq M_5 > M_2$. The largest difference in affinity was below ten times (between M_4 and M_5 for 3-MPB and between M_2 and M_4 for 4-MPB). These competition binding data of (+)3- and 4-MPB showed that neither of these substances has an affinity profile that makes them suitable for subtype-specific assays [26].

3.2 In Vivo Assessment of ^{11}C-(+)3-MPB Analogs

^{11}C-(+)3-MPB and its *N*-alkyl substitution analogs, (−)3-MPB, (+) and (−)3-EPB, (+) and (+)3-EPB, were labeled by using ^{11}C-methyl iodide, ^{11}C-ethyl iodide, or ^{11}C-propyl iodide for the alkylation of (+) or (−)3-PB as shown in Fig. 2. Each of these compounds was intravenously injected into monkey for scanning for 90 min, and then the acquired data were reconstructed to images for TAC determination as sequential images and ROI setting as summation images from 60 to 90 min after the injection.

In Fig. 3, typical PET images of ^{11}C-(+)3-MPB (B), ^{11}C-(−)3-MPB (C), ^{11}C-(+)3-EPB (D), ^{11}C-(+)3-PPB (E), and ^{11}C-4-MPB (A) as a reference are shown, which were obtained from the same monkey under conscious condition. The regional uptake pattern of ^{11}C-(+)3-MPB was high in the striatum; intermediate in the

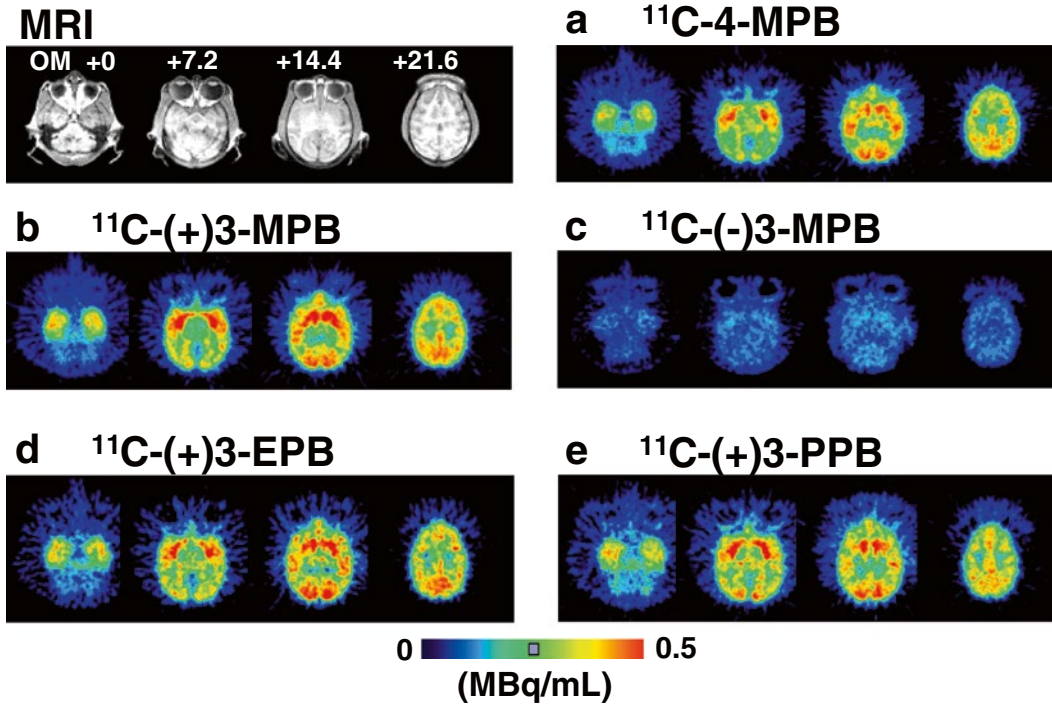

Fig. 3 MRI and PET images of ^{11}C-4-MPB (**a**), ^{11}C-(+)3-MPB (**b**), ^{11}C-(−)3-MPB (**c**), ^{11}C-(+)3-EPB (**d**), and ^{11}C-(+)3-PPB (**e**) in conscious monkey brain. PET data were collected in the conscious state with a high-resolution PET scanner (HAMAMATSU SHR-7700) with transaxial special resolution of 2.6 mm (FWHM). Each labeled compound (100–120 MBq/kg body weight) was injected through the venous cannula. PET scans were performed for 91 min, and each PET image was generated by summation of image data from 60 to 94 min post-injection

occipital, temporal, and frontal cortices, hippocampus, and thalamus; and low in the cerebellum (Fig. 3b). In contrast, the level of ^{11}C-(−)3-MPB was much lower than those of ^{11}C-(+)3-MPB showing a homogeneous distribution in all regions of the brain (Fig. 3c). The patterns of distribution of ^{11}C-(+)3-EPB (Fig. 3d), ^{11}C-(+)3-PPB (Fig. 3e), and ^{11}C-4-MPB (Fig. 3a) were almost identical to that of ^{11}C-(+)3-MPB. There results demonstrated that specificity of these PET probes except ^{11}C-(−)3-MPB remained constant even upon substitution of *N*-alkyl moiety.

The time activity curves of ^{11}C-(+)3-MPB in the frontal, temporal, and occipital cortices reached their peaks 40 min after injection, whereas the striatal and hippocampal regions reached peak values 60 min after injection. In contrast, the time–activity curves of ^{11}C-(−)3-MPB showed similar patterns in all regions of the brain [19]. The uptake of ^{11}C-4-MPB in all regions except the thalamus and cerebellum gradually increased over time during the scan until 91 min after injection [19].

As shown in Fig. 4a, Patlak plot graphical analysis demonstrated that ^{11}C-(+)3-MPB provided nonlinear curves showing slope = 0 in the late phase, suggesting that the dissociation rate constant (k_4) from mAChR was not negligible. Next, Logan plot graphical analysis was applied to investigate the in vivo binding of ^{11}C-(+)3-MPB (Fig. 4b). The ratio of Logan slopes (DV) of ^{11}C-(+)3-MPB in each region against the cerebellum was

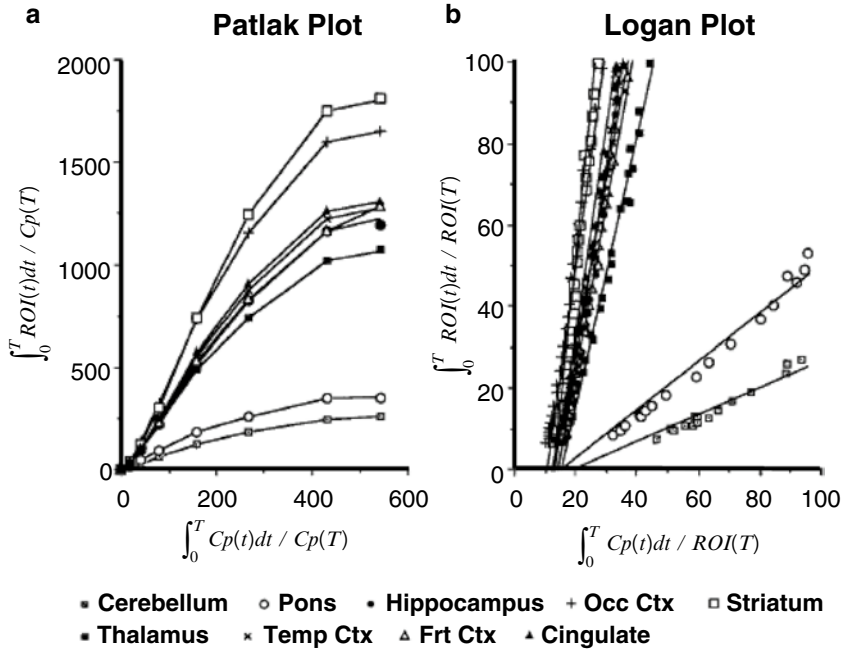

Fig. 4 Patlak plot graphical (**a**) and Logan plot graphical analysis (**b**) of ^{11}C-(+)3-MPB in conscious monkey brain. Regions of interest (ROIs) were identified according to an MRI scan of the each animal, and metabolite-corrected plasma input was applied for quantitative measurements of ^{11}C-(+)3-MPB binding to mAChR in the living brain

correlated with the data of mAChR density (B_{MAX}) as measured by the in vitro assay [48]. These results demonstrated that ^{11}C-(+)3-MPB was a more suitable PET probe for the quantification of mAChR in the living brain than conventional ^{11}C-labeled ligands such as ^{11}C-4-MPB and ^{11}C-scopolamine.

As described in Section 3.1, two *N*-alkyl substitution analogs of (+)3-MPB, (+)3-EPB, and (+)3-PPB revealed lower affinities to mAChR than 4-MPB and (+)3-MPB. In order to develop PET probes with moderate affinity to assess neurotransmitter release into the synaptic cleft [29, 43, 49], we attempted to synthesize ^{11}C-(+)3-EPB and ^{11}C-(+)3-PPB, and evaluated their specificity and kinetics in comparison with those of original ^{11}C-(+)3-MPB in conscious monkey brain.

The time–activity curves demonstrated that the peak times shifted to an earlier time with a higher clearance rate after injection of PET probes with longer ^{11}C-alkyl chains [18]. As shown in Fig. 5, kinetic analysis indicated that labeling with a longer ^{11}C-alkyl chain induced lower binding potential (Frontal cortex; 2.4, 2.0, and 1.4 for ^{11}C-(+)3-MPB, ^{11}C-(+)3-EPB, and ^{11}C-(+)3-PPB, respectively). The administration of Aricept, an AChE inhibitor, increased acetylcholine level in extracellular fluid of the frontal cortex (ca. 150 % and 175 % of baseline at 50 μg/kg and 250 μg/kg, respectively) [18]. The binding of ^{11}C-(+)3-PPB with the lowest affinity to mAChR was displaced by the endogenous ACh induced by Aricept, while ^{11}C-(+)3-MPB with the highest affinity was not significantly affected (Fig. 5). These results suggested that increasing ^{11}C-alkyl chain length did alter the kinetic properties of PET probes by reducing the affinity to mAChR, which might make it possible to assess the interaction between the endogenous neurotransmitter acetylcholine and ligand-receptor binding in vivo as measured by PET.

3.3 Effects of Aging on mAChR

In aged monkeys, the time–activity curves of ^{11}C-(+)3-MPB in regions rich in mAChR peaked at earlier time points with faster elimination rates than those in young monkeys, while curves in the cerebellum showed no significant difference between young and aged animals [20]. Significant age-related alterations of the in vivo binding of ^{11}C-(+)3-MPB were observed in the temporal and frontal cortices and the striatum (Fig. 6a). The Scatchard plot revealed a linear curve for ^{11}C-(+)3-MPB in all regions of young and aged monkeys (Fig. 6b). Aged animals showed the age-related reduction in the maximum number of binding sites (B_{MAX}) of mAChR, while there was no age-related alteration in the affinity ($1/K_D$) of mAChR for (+)3-MPB (Fig. 6b).

Previous studies demonstrated, when expressed relative to the cerebellum, which is assumed to be a nonspecific and tracer-free reference region, age-related reduction of mAChR in almost all cerebral regions in humans as measured by ^{11}C-benztropine [37] and ^{11}C-4-MPB [38–40]. There were trends toward reduced cerebral mAChR binding and toward elevated cerebellar binding with aging in humans,

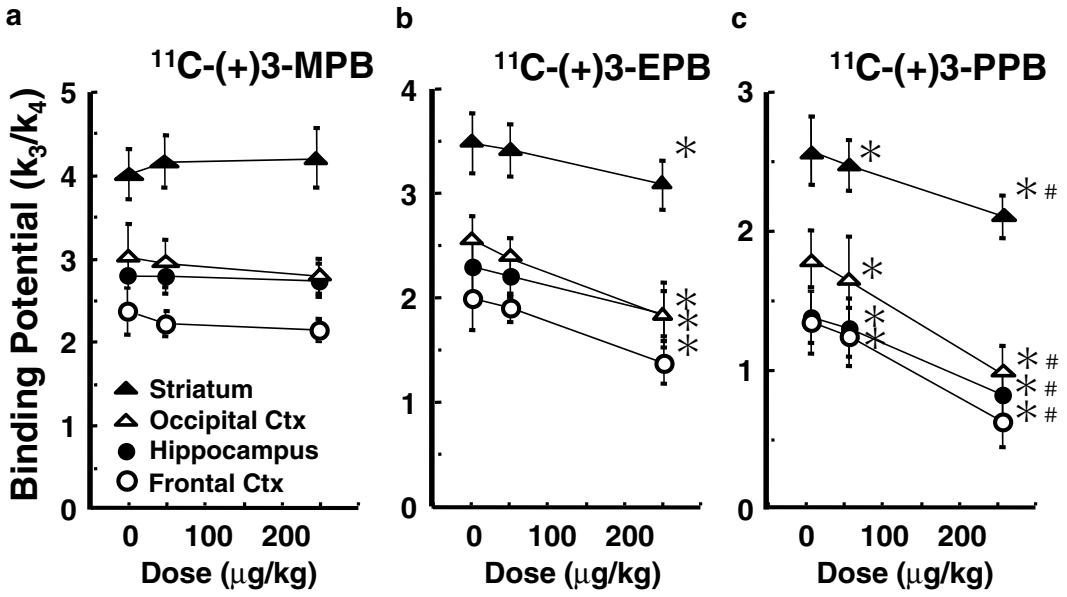

Fig. 5 Dose-dependent effects of Aricept on the binding of ^{11}C-(+)3-MPB (**a**), ^{11}C-(+)3-EPB (**b**), and ^{11}C-(+)3-PPB (**c**) to mAChR in the cortical regions of conscious monkey brain. PET scans were performed as shown in the legend of Fig. 3. Data are expressed as means ± SD for five animals per treatment condition. *$P < 0.01$ vs. saline. #$P < 0.01$ vs. 50 μg/kg Aricept

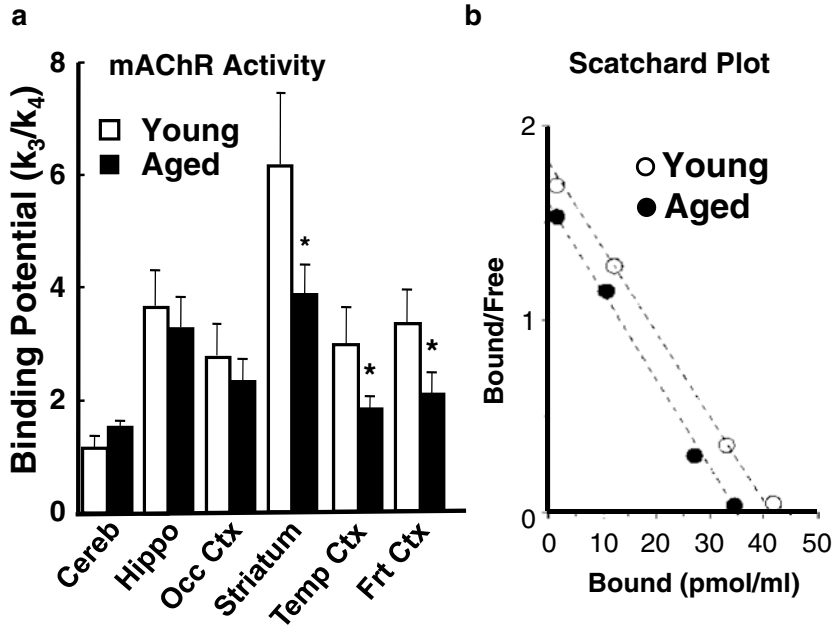

Fig. 6 Age-related changes in cerebral mAChR binding in vivo as measured with ^{11}C-(+)3-MPB. (**a**) PET scans in young (ca. 6 years old) and aged (ca. 20 years old) monkeys were performed as shown in the legend of Fig. 3. Data represent means ± SD for seven animals per group. *$P < 0.05$ vs. young animals. (**b**) Scatchard plot analysis was conducted by injection of carrier-free ^{11}C-(+)3-MPB, and together with various amounts of cold (+)3-MPB to measure in vivo binding parameters (B_{MAX} and K_D)

as measured by a kinetic analysis method using ^{11}C-tropanyl benzilate using metabolite-corrected plasma TAC as input function, a gold standard kinetic analysis for reliable quantification of receptor binding in vivo [41]. This may suggest when used cerebellar TAC as input function, the opposing cortical and cerebellar changes of binding led to the apparent age-related loss of mAChR binding.

3.4 mAChR Occupancy and Cognition

With applying T-DMS task test, the memory assessment of young monkeys was serially conducted 2, 6, 24 and 48 h after administration of scopolamine at the doses of 10 and 30 μg/kg. Scopolamine impaired the memory performance in a dose-dependent manner 2 h after administration, followed by gradual recovery at 24 h and later after scopolamine administration (Fig. 7b). The time-dependent

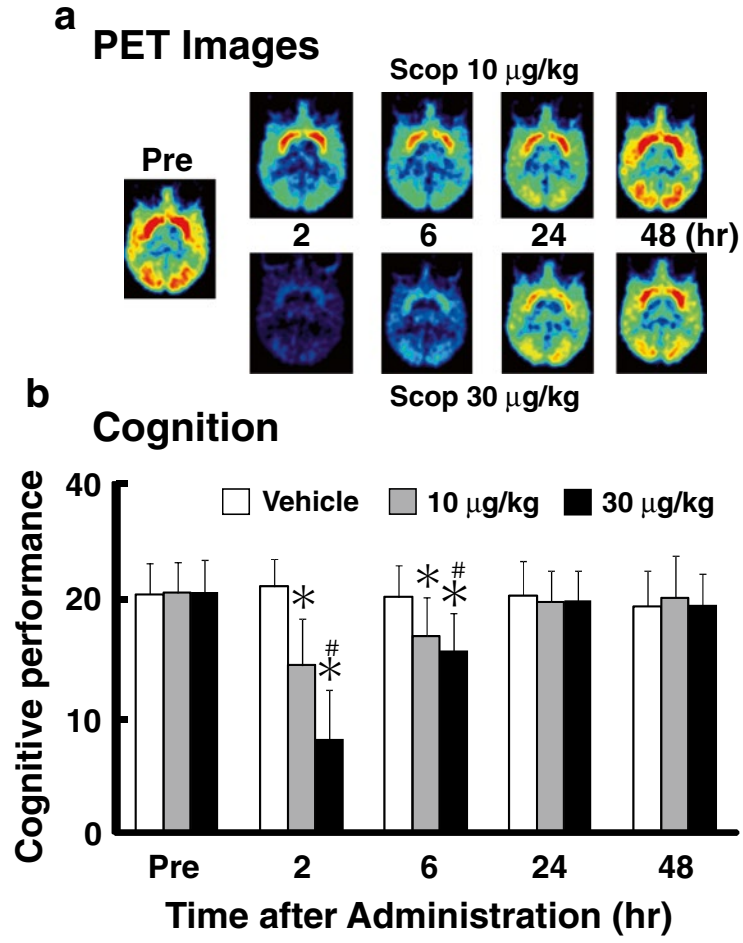

Fig. 7 Effects of scopolamine on ^{11}C-(+)3-MPB binding in conscious monkey brain (**a**) and on titration-delayed match to sample (T-DMS) task (**b**). Time courses of the mAChR occupancy (**a**) and cognitive index (**b**) were serially monitored 2, 6, 24, and 48 h after the administration of vehicle or scopolamine at doses of 10 and 30 μg/kg. $^{*}P < 0.01$ vs. saline. $^{\#}P < 0.01$ vs. 0.01 mg/kg scopolamine

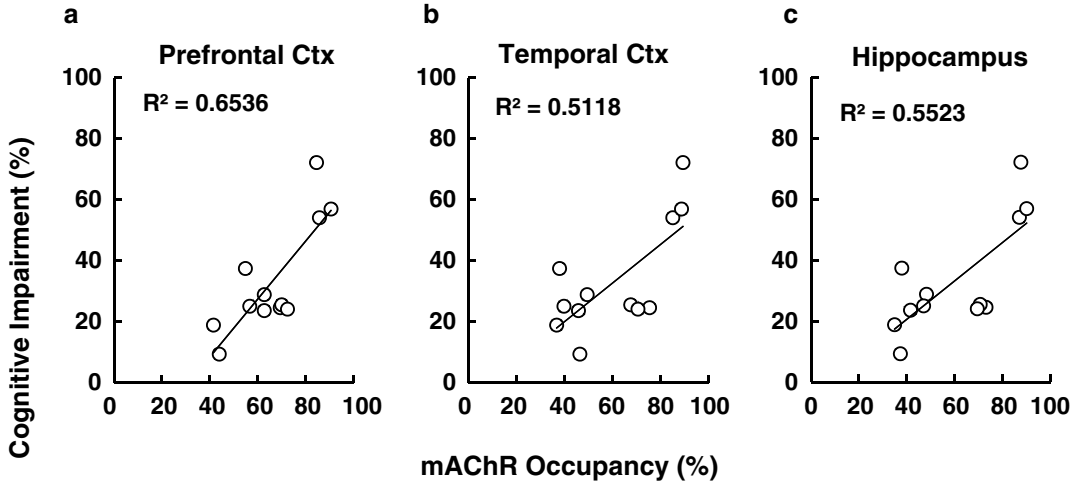

Fig. 8 Relationship between mAChR occupancy and cognitive impairment. Occupancy levels in prefrontal cortex (**a**), temporal cortex (**b**), and hippocampus (**c**) were assessed 2 and 6 h after scopolamine administration at the doses of 10 and 30 μg/kg

changes in occupancy of mAChR by scopolamine were simultaneously observed with serial PET measurements using ^{11}C-(+)3-MPB. Occupancy levels of mAChR peaked 2 h after scopolamine administration in the cortical regions innervated primarily by the basal forebrain, thalamus, and brainstem (Fig. 7a). As shown in Fig. 8, mAChR occupancy and the degree of cognitive impairment were significantly and positively correlated in the brain regions assessed. Cognitive impairment induced by scopolamine persisted for 6 h and was followed by complete recovery to normal levels 24 h later. It was very interesting that some scopolamine binding to mAChRs was still observed in most brain areas except the brainstem 24 h after scopolamine administration, suggesting the existence of a threshold (ca. 25 %) of mAChR occupancy to induce cognitive impairment.

4 Limitations

All these data described above indicate that ^{11}C-(+)3-MPB [17, 19] is superior to its previous alternatives, such as ^{11}C-scopolamine [8–10], ^{11}C-QNB [12], ^{11}C-dexetimide [11], ^{11}C-benztropine [13], ^{11}C-TRB [14, 15], and ^{11}C-4-MPB [16]. However, several limitations of ^{11}C-(+)3-MPB remain to be solved. One limitation may be poor subtype selectivity for mAChR, which consist of at least the M_1–M_5 subtypes. The in vitro radioligand binding experiments performed with five cloned human mAChR subtypes expressed in CHO-K1 cells demonstrated that (+)3-MPB have no apparent selectivity for M_1 and M_2 receptors (unpublished data), suggesting that ^{11}C-(+)3-MPB images the integration of both M_1

and M_2 receptors. To compensate the poor selectivity, a selective agonist-based PET probe for M_2 receptor, 3-(3-(3-^{18}F-flouropropyl) thio)-1,2,5-thiadiazol-4-yl)-1,2,5,6-tetrahydro-1-methylpyridine (^{18}F-FP-TZTP) was developed with K_i of 2.2 and 7.4 nM for M_2 and M_1, respectively [50]. By using mice with the knocked-out M_1, M_2, M_3, or M_4 receptors, it was confirmed that ^{18}F-FP-TZTP selectively bound to M_2 mAChR subtype [51].

The assessment of neurotransmitter release in the living brain should be very important from neurological and pharmacological points of view. In the last decade, interactions between endogenous neurotransmitters released into the synaptic cleft and the binding of labeled compounds have been examined by neuroimaging with PET/SPECT, especially in the dopaminergic system [29, 43, 49]. As demonstrated with ^{11}C-(+)3-EPB and ^{11}C-(+)3-PPB [18], the cortical binding of ^{18}F-FP-TZTP was also decreased by physostigmine, a AChE inhibitor, showing the competition between ^{18}F-FP-TZTP and increased synaptic endogenous ACh on mAChRs [52]. This PET probe seemed to be more favorable than previous ones; however uncertain properties have been revealed on ^{18}F-FP-TZTP as described later.

There is a loss of cholinergic neurons in the forebrain, reduced cholinergic activity in the hippocampus, and cortical loss of choline acetyltransferase in AD, and the severity of these cholinergic abnormalities is correlated well with the degree of dementia [3–7]. Noninvasive imaging of mAChRs in the brain could contribute to the diagnosis and monitoring of medications for treatment of these diseases. Of interest, an age-related "increased" binding of agonist-based ^{18}F-FP-TZTP was determined [53], which was completely the opposite result obtained with antagonist-based ^{11}C-benztropine [37], ^{11}C-4-MPB [38–40], ^{11}C-tropanyl benzilate [41], and ^{11}C-(+)3-MPB [20], showing "decreased" binding. The authors speculated that a lower concentration of ACh in the synapse was one possible explanation for the age-related increase in ^{18}F-FP-TZTP binding [53]. It remains controversial that opposite effects of aging on mAChR binding were observed between agonist-based and antagonist-based PET probes. We reported the similar opposite effects of stress induced by head motion restriction on dopamine D_2 receptor binding between agonist-based (^{11}C-MNPA) and antagonist-based PET probes (^{11}C-raclopride) [34]. Although it is well established that agonists can bind to a "high-affinity" state of the receptor, this phenomenon is conceptually unresolved because it has yet to be ascertained exactly what state of the receptor (conformational, coupled etc.) defines "high-affinity." These results suggest that when we attempt to develop novel PET probes, we should take into account the chemical properties of agonist or antagonist.

5 Conclusion

This chapter has introduced the procedure how to develop the novel PET probes for quantitative mAChR imaging with PET, and also showed how to utilize these PET probes in preclinical and clinical researches based on our own experiences. Thus, we developed novel PET probes for mAChR imaging, ^{11}C-(+)3-MPB and its *N*-alkyl substitution analogs with suitable kinetic properties for quantitative imaging of mAChRs in the living brain with PET. On the basis of these preclinical evaluations of ^{11}C-(+)3-MPB as a novel PET probe for mAChR imaging, we applied this PET probe to assess the changes in mAChR binding in the brain of chronic fatigue syndrome patients [54]. These results of our studies described in this chapter strongly suggested the usefulness of these PET probes for pathophysiological and neurological assessments of neurological/mental disorders.

References

1. Katzman R (1986) Alzheimer's disease. N Engl J Med 314:964–973
2. Selkoe DJ (1990) Deciphering Alzheimer's disease: the amyloid precursor protein yields new clues. Science 248:1058–1060
3. Höhmann C, Antuono P, Coyle JT (1998) Basal forebrain cholinergic neurons and Alzheimer's disease. In: Iversen LL, Iversen SD, Snyder SD (eds) Psychopharmacology of the aging nervous system. Plenum, New York, pp 69–106
4. Perry EK (1986) The cholinergic hypothesis—ten years on [Review]. Br Med Bull 42:63–69
5. Rinne JO, Laakso K, Lönnberg P et al (1985) Brain muscarinic receptors in senile dementia. Brain Res 336:19–25
6. Reinikainen KJ, Riekkinen PJ, Halonen T et al (1987) Decreased muscarinic receptor binding in cerebral cortex and hippocampus in Alzheimer's disease. Life Sci 41:453–461
7. Terry AV Jr, Buccafusco JJ (2003) The cholinergic hypothesis of age and Alzheimer's disease-related cognitive deficits: recent challenges and their implications for novel drug development. J Pharmacol Exp Ther 306:821–827
8. Vora MM, Finn RD, Boothe TE (1983) [*N*-methyl-^{11}C]Scopolamine: synthesis and distribution in rat brain. J Labelled Comp Radiopharm 20:1229–1234
9. Mulholland GK, Jewett DW, Toorongian SA (1988) Routine synthesis of *N*-[^{11}C-methyl] scopolamine by phosphate mediated reductive methylation with [^{11}C]formaldehyde. Appl Radiat Isot 39:373–379
10. Frey KA, Koeppe RA, Mulholland GK et al (1992) *In vivo* muscarinic cholinergic receptor imaging in human rain with [^{11}C]scopolamine and positron emission tomography. J Cereb Blood Flow Metab 12:147–1541
11. Dannals RF, Långström B, Ravert HT et al (1988) Synthesis of radiotracers for studying muscarinic cholinergic receptors in the living human brain using positron emission tomography: [^{11}C]dexetimide and [^{11}C]levetimide. Appl Radiat Isot 39:291–295
12. Prenant C, Barre L, Crouzel C (1989) Synthesis of n.c.a. [^{11}C]QNB. J Labelled Comp Radiopharm 26:199–201
13. Dewey SL, MacGregor RR, Brondie JD et al (1990) Mapping muscarinic receptors in human and baboon brain using [N^{11}C-methyl]benztropine. Synapse 5:213–223
14. Mulholland GK, Otto CA, Jewett DW et al (1992) Synthesis, rodent biodistribution, dosimetry, metabolism and monkey images of carbon-11-labeled (+)-2α-tropanyl benzilate: a central muscarinic receptor imaging agent. J Nucl Med 33:423–430
15. Koeppe RA, Frey KA, Mulholland GK et al (1994) [^{11}C]Tropanyl benzilate binding to muscarinic cholinergic receptors: methodology and kinetic modeling alterations. J Cereb Blood Flow Metab 14:85–99
16. Zubieta JK, Koeppe RA, Mulholland GK et al (1998) Quantification of muscarinic cholinergic receptors with [^{11}C]NMPB and positron emission tomography: method development and differentiation of tracer delivery from

receptor binding. J Cereb Blood Flow Metab 18:619–631

17. Takahashi K, Murakami M, Miura S et al (1999) Synthesis and autoradiographic localization of muscarinic cholinergic antagonist *N*-^{11}C-methyl-3-piperidyl benzilate as a potent radioligand for positron emission tomography. Appl Radiat Isot 50:521–525
18. Nishiyama S, Tsukada H, Sato K et al (2001) Evaluation of PET ligands (+)N-[^{11}C]ethyl-3-piperidyl benzilate and (+)*N*-[^{11}C]propyl-3-piperidyl benzilate for muscarinic cholinergic receptors: a PET study with microdialysis in comparison with (+)*N*-[^{11}C]methyl-3-piperidyl benzilate in the conscious monkey brain. Synapse 40:159–169
19. Tsukada H, Takahashi K, Miura S et al (2001) Evaluation of novel PET ligands (+)*N*-[^{11}C] methyl-3-piperidyl benzilate ([^{11}C](+)3-MPB) and its stereoisomer [^{11}C](−)3-MPB for muscarinic cholinergic receptors in the conscious monkey brain: a PET study in comparison with [^{11}C]4-MPB. Synapse 39:182–192
20. Tsukada H, Kakiuchi T, Nishiyama S et al (2001) Age differences in muscarinic cholinergic receptors assayed with (+)*N*-[^{11}C]methyl-3-piperidyl benzilate in the brains of conscious monkeys. Synapse 41:248–257
21. Tsukada H, Nishiyama S, Fukumoto D et al (2004) Effects of acute acetylcholinesterase inhibition on the cerebral cholinergic neuronal system and cognitive function: functional imaging of the conscious monkey brain using animal PET in combination with microdialysis. Synapse 52:1–10
22. Yamamoto S, Nishiyama S, Kawamata M et al (2011) Muscarinic receptor occupancy and cognitive impairment: A PET study with [^{11}C](+)3-MPB and scopolamine in conscious monkeys. Neuropsychopharmacology 36:1455–1465
23. Biel JH, Abood LG, Hoya WK et al (1961) Central stimulant. II, Cholinergic blocking agents. J Org Chem 26:4096–4103
24. Cheng YC, Prusoff WH (1973) Relationship between the inhibition constant (Ki) and the concentration of inhibitor which causes 50 percent inhibition (IC_{50}) of an enzymatic reaction. Biochem Pharmacol 22:3099–3108
25. Paxinos G, Watson C (1982) The rat brain in stereotaxic coordinates. Academic, New York
26. Sihver S (2000) Development of in vitro and ex vivo positron-emitting tracer techniques and their application to neurotrauma. Thesis in Faculty of Medicine, Uppsala University
27. Långström B, Antoni G, Gullberg P et al (1986) The synthesis of L-^{11}C-labeled ethyl, propyl, butyl and isobutyl iodides and examples of alkylation reactions. Appl Radiat Isot 37: 1141–1145
28. Irie T, Fukushi K, Namba H et al (1996) Brain acetylcholinesterase activity: validation of a PET tracer in a rat model of Alzheimer's disease. J Nucl Med 37:649–655
29. Tsukada H, Harada N, Nishiyama S et al (2000) Ketamine decreased striatal [^{11}C]raclopride binding with no alteration in static dopamine concentrations in the striatal extracellular fluid in the monkey brain: Multi-parametric PET studies combined with microdialysis analysis. Synapse 37:95–103
30. Tsukada H, Nishiyama S, Kakiuchi T et al (2001) Ketamine alters the availability of striatal dopamine transporter as measured by [^{11}C] β-CFT and [^{11}C]β-CIT-FE in the monkey brain. Synapse 42:273–280
31. Tsukada H, Miyasato K, Kakiuchi T et al (2002) Comparative effects of methamphetamine and nicotine on the striatal [^{11}C]raclopride binding in unanesthetized monkeys. Synapse 45:207–212
32. Ohba H, Harada N, Nishiyama S et al (2009) Ketamine/xylazine anesthesia alters [^{11}C] MNPA binding to dopamine D_2 receptors and response to methamphetamine challenge in monkey brain. Synapse 63:534–537
33. Watanabe M, Okada H, Shimizu K et al (1997) A high resolution animal PET scanner using compact PS-PMT detectors. IEEE Trans Nucl Sci 44:1277–1282
34. Tsukada H, Ohba H, Nishiyama S et al (2011) Differential effects of stress on [^{11}C]raclopride and [^{11}C]MNPA binding to striatal D_2/D_3 dopamine receptors: a PET study in conscious monkeys. Synapse 64:84–89
35. Logan J, Fowler J, Volkow N et al (1990) Graphical analysis of reversible radioligand binding from time-activity measurements applied to *N*-^{11}C-methyl-(−)-cocaine PET studies in human subjects. J Neurochem 10: 740–747
36. Patlak C, Blasberg RG, Fenstermacher JD (1983) Graphical evaluation of blood-to-brain transfer constants from multiple-time uptake data. J Cereb Blood Flow Metab 3:1–7
37. Dewey SL, Volkow ND, Logan J et al (1990) Age-related decrease in muscarinic cholinergic receptor binding in the human brain measured with positron emission tomography (PET). J Neurosci Res 27:569–575
38. Suhara T, Inoue O, Kobayashi K et al (1993) Age-related changes inhuman muscarinic acetylcholine receptors measured by positron emission tomography. Neurosci Lett 149: 225–228

39. Yoshida T, Kuwabara Y, Ichiya Y et al (1998) Cerebral muscarinic acetylcholinergic receptor measurement in Alzheimer's disease patient on 11C-methyl-4-piperidyl benzilate—comparison with cerebral blood flow and cerebral glucose metabolism. Ann Nucl Med 12:35–42
40. Zubieta JK, Koeppe RA, Frey KA et al (2001) Assessment of muscarinic receptor concentrations in aging and Alzheimer disease with ^{11}C-NMPB and PET. Synapse 39:275–287
41. Lee KS, Frey KA, Koeppe RA et al (1996) *In vivo* quantification of cerebral muscarinic receptors in normal human aging using positron emission tomography and [^{11}C]tropanyl benzilate. J Cereb Blood Flow Metab 16: 303–310
42. Tsukada H, Kreuter J, Maggos CE et al (1996) Effects of binge pattern cocaine administration on dopamine D_1 and D_2 receptors in the rat brain: an *in vivo* study using positron emission tomography. J Neurosci 16:7670–7677
43. Tsukada H, Harada N, Nishiyama S et al (2000) Cholinergic neuronal modulation alters dopamine D_2 receptor availability in vivo by regulating receptor affinity induced by facilitated synaptic dopamine turnover: PET studies with microdialysis in the conscious monkey brain. J Neurosci 20:7067–7073
44. Scatchard G (1949) The attractions of proteins for small molecules and ions. Ann N Y Acad Sci 51:660–672
45. Collerton D (1986) Cholinergic function and intellectual decline in Alzheimer's disease [Review]. Neuroscience 19:1–28
46. Hudzik TJ, Wenger GR (1993) Effects of drugs of abuse and cholinergic agents on delayed matching-to-sample responding in the squirrel monkey. J Pharmacol Exp Ther 265: 120–127
47. Tejani-Butt SM, Luthin GR, Wolfe BB et al (1990) *N*-substituted derivatives of 4-piperidinyl benzilate: affinities for brain muscarinic acetylcholine receptors. Life Sci 47:841–848
48. Snyder SH, Chang KJ, Kuhar MJ et al (1975) Biochemical identification of the mammalian muscarinic cholinergic receptor. Fed Proc 34:1919–1921
49. Laruelle M (2000) Imaging synaptic neurotransmission with in vivo binding competition techniques: a critical review. J Cereb Blood Flow Metab 20:423–451
50. Kiesewetter DO, Lee J, Lang L et al (1995) Preparation of ^{18}F-labeled muscarinic agonist with M_2 selectivity. J Med Chem 38:5–8
51. Jagoda EM, Kiesewetter DO, Shimoji K et al (2003) Regional brain uptake of the muscarinic ligand, [^{18}F]FP-TZTP, is greatly decreased in M_2 receptor knockout mice but not in M_1, M_3 and M_4 receptor knockout mice. Neuropharmacology 44:653–661
52. Carson RE, Kiesewetter DO, Jagoda E et al (1998) Muscarinic cholinergic receptor measurements with [^{18}F]FP-TZTP: control and competition studies. J Cereb Blood Flow Metab 18:1130–1142
53. Podruchny TA, Connolly C, Bokde A et al (2003) In vivo muscarinic 2 receptor imaging in cognitively normal young and older volunteers. Synapse 48:39–44
54. Yamamoto S, Ouchi Y, Nakatsuka D et al (2012) Reduction of [^{11}C](+)3-MPB binding in brain of chronic fatigue syndrome with serum autoantibody against muscarinic cholinergic receptor. PLoS One 7, e51515